JCI insight

RESEARCH ARTICLE

Metabolite profiling identifies anandamide as a biomarker of nonalcoholic steatohepatitis

W. Taylor Kimberly,[1] John F. O'Sullivan,[2] Anjali K. Nath,[3] Michelle Keyes,[4] Xu Shi,[2] Martin G. Larson,[4,5] Qiong Yang,[4,5] Michelle T. Long,[4,6] Ramachandran Vasan,[4] Randall T. Peterson,[3] Thomas J. Wang,[7] Kathleen E. Corey,[8] and Robert E. Gerszten[2]

[1]Center for Genomic Medicine, Department of Neurology, Massachusetts General Hospital, Boston, Massachusetts, USA. [2]Division of Cardiovascular Medicine, Beth Israel Deaconess Hospital, Boston, Massachusetts, USA. [3]Division of Cardiology, Department of Medicine, Massachusetts General Hospital, Boston, Massachusetts, USA. [4]Framingham Heart Study of the National Heart, Lung, and Blood Institute and Boston University School of Medicine, Framingham, Massachusetts, USA. [5]Biostatistics Department, Boston University School of Public Health, Boston, Massachusetts, USA. [6]Section of Gastroenterology, Department of Medicine, Boston University School of Medicine, Boston, Massachusetts, USA. [7]Division of Cardiovascular Medicine, Department of Medicine, Vanderbilt University, Nashville, Tennessee, USA. [8]Division of Gastroenterology, Department of Medicine, Massachusetts General Hospital, Boston, Massachusetts, USA.

The discovery of metabolite-phenotype associations may highlight candidate biomarkers and metabolic pathways altered in disease states. We sought to identify novel metabolites associated with obesity and one of its major complications, nonalcoholic fatty liver disease (NAFLD), using a liquid chromatography–tandem mass spectrometry method. In 997 individuals in Framingham Heart Study Generation 3 (FHS Gen 3), we identified an association between anandamide (AEA) and BMI. Further examination revealed that AEA was associated with radiographic hepatic steatosis. In a histologically defined NAFLD cohort, AEA was associated with NAFLD severity, the presence of nonalcoholic steatohepatitis, and fibrosis. These data highlight AEA as a marker linking cardiometabolic disease and NAFLD severity.

Introduction

Nonalcoholic fatty liver disease (NAFLD) is characterized by histology or imaging-defined hepatic steatosis, in the absence of secondary causes (1). NAFLD comprises a spectrum of pathology, ranging from steatosis to nonalcoholic steatohepatitis (NASH), which is a progressive form of NAFLD that can advance to cirrhosis and hepatocellular carcinoma (1). The development of NAFLD is linked to elevated BMI, central obesity, and the cardiometabolic syndrome (2, 3). Moreover, NAFLD may be a predictor for the development of diabetes mellitus and is an independent risk factor for cardiovascular disease (4, 5). Although NAFLD is connected to metabolic derangements associated with obesity, the pathways that link NAFLD, obesity, and cardiometabolic disease are poorly understood.

Metabolite profiling is an approach that has previously identified novel associations in diabetes mellitus and other cardiometabolic diseases in large community-based cohorts (6–11). To further elucidate the metabolic links among obesity, cardiometabolic disease, and NAFLD, we developed a metabolite-profiling method that detects both positively and negatively charged analytes from a single sample preparation. Coupling amide chromatography (12) and tandem mass spectrometry (13), we optimized conditions for profiling of human plasma samples.

Using this metabolite-profiling method, we evaluated the association between metabolites and cardiometabolic traits in the Framingham Heart Study Generation 3 (FHS Gen 3) cohort. We identified anandamide (AEA) as a candidate metabolite for cardiometabolic traits and then extended our findings in a hospital-based NAFLD cohort that demonstrated that AEA was associated with NAFLD severity. Cumulatively, these studies identify AEA as a candidate biomarker linking obesity and NAFLD.

Conflict of interest: The authors have declared that no conflict of interest exists.

Submitted: January 23, 2017
Accepted: April 4, 2017
Published: May 4, 2017

Reference information:
JCI Insight. 2017;2(9):e92989. https://doi.org/10.1172/jci.insight.92989.

Table 1. Characteristics of Framingham Heart Study Generation 3 participants at exam 1

Variable	*n* = 997
Age, yr (mean ± SD)	40 ± 9
Female, *n* (%)	526 (53%)
BMI, kg/m^2 (mean ± SD)	26.6 ± 5.3
Waist, inches (mean ± SD)	36.3 ± 5.7
SBP, mmHg(mean ± SD)	117 ± 14
DBP, mmHg (mean ± SD)	75 ± 9
HOMA-IR (mean ± SD)	1.04 ± 0.83
Glucose, mg/dl (mean ± SD)	96 ± 19
HDL, mg/dl (mean ± SD)	60 ± 18
Triglycerides, mg/dl (mean ± SD)	109 ± 66
Creatinine, mg/dl (mean ± SD)	0.80 ± 0.15

SBP, systolic blood pressure; DBP, diastolic blood pressure; HOMA-IR, homeostatic model assessment of insulin resistance.

Results

Metabolites associated with cardiometabolic traits in the Framingham Heart Study. Using a multifunctional approach that detects both positively and negatively charged metabolites, we developed a metabolite-profiling method that assessed 179 analytes across important metabolic pathways (see Supplemental Methods for details; supplemental material available online with this article; https://doi.org/10.1172/jci.insight.92989DS1). We analyzed plasma samples of 997 participants in FHS Gen 3, a longitudinal, community-based study that began enrollment in 2002. The clinical characteristics of the cohort are shown in Table 1. Participants had no overt cardiovascular disease, had a mean age of 40 ± 9 years, a BMI of 26.6 ± 5.3 kg/m^2, and a homeostatic model assessment of insulin resistance (HOMA-IR) value of 1.04 ± 0.83.

In regression analyses adjusted for age and sex, we assessed metabolite associations with cardiometabolic traits, including generalized obesity, as measured by BMI; central obesity, as assessed by waist circumference (WC); and glucose metabolism, as assessed by fasting glucose level and HOMA-IR. Associations that exceeded the Bonferroni-corrected *P* value threshold are presented in Table 2. The full set of associations across cardiometabolic phenotypes, which included systolic and diastolic blood pressure, HDL, and triglycerides, is further presented in Supplemental Tables 2–9.

Several known associations with obesity and insulin metabolism were validated, including uric acid (14); 2-aminoadipic acid (15); glutamate (16); the branched-chain amino acids leucine, isoleucine, and valine (17, 18); the short-chain acyl carnitines C3- and C6-carnitine (18); the tryptophan catabolite kynurenic acid (16); and amino acids tyrosine, alanine, and glycine (17). We also identified associations with metabolites that map to pathways previously associated with cardiometabolic disease, including the branched-chain ketoacid 2-ketoisovaleric acid and the tryptophan catabolites quinolinic acid, xanthurenic acid, indole-3-propionic acid, and kynurenine. Intermediate products of purine degradation and uric acid production included inosine, hypoxanthine, and xanthine. Several analytes that spanned glucose metabolism and the tricarboxylic acid cycle were elevated, including glucose, lactic acid, pyruvic acid, α-ketoglutaric acid, aconitic acid, and malic acid. Taken together, the identification of known metabolite-phenotype associations and pathways confirmed the validity of our approach.

AEA and associations with obesity and cardiometabolic traits. In the FHS Gen 3, analytes associated with cardiometabolic disease traits included uridine diphosphate *N*-acetylglucosamine (UDP-GlcNAc), reduced glutathione, hippuric acid, and AEA (see Table 2). Of these four candidates, AEA was notable for its association across metabolic traits, including generalized and central obesity and glucose metabolism, with the greatest association with markers of obesity. Linear regression with BMI yielded an adjusted β coefficient of 0.22 ($P = 3.6 \times 10^{-13}$); for WC, the age- and sex-adjusted β coefficient was 0.20 ($P = 1.6 \times 10^{-12}$). In age- and sex-adjusted logistic regression analyses, for each unit increase in AEA, the odds ratio (OR) for obesity (defined as BMI ≥ 30) was 3.20 (95% CI 2.10–4.88, $P = 6.3 \times 10^{-8}$) and for excessive WC (defined as ≥88 cm), the OR was 2.79 (95% CI 1.85–4.20, $P = 9.2 \times 10^{-7}$). AEA was also associated with elevated fasting serum glucose (glucose >110 mg/dl; OR 3.12, 95% CI 1.80–5.40, $P = 4.9 \times 10^{-5}$) and abnormal HOMA-IR (HOMA-IR ≥2.0, OR 2.16, 95% CI 1.51–3.09, $P = 2.5 \times 10^{-5}$) after adjustment for age and sex.

We sought to extend our work on AEA by assessing for associations with NAFLD, an obesity-related phenotype. Prior animal studies have suggested that the putative AEA receptor CB1 may modulate the accumulation of hepatic fat (19, 20), and a recent case-control cohort study identified an association between the endocannabinoid system and NAFLD (21). We therefore assessed for an association between AEA and radiographic hepatic steatosis in the FHS Gen 3 cohort and found an age- and sex-adjusted β coefficient of –0.013 ($P = 0.03$).

AEA levels correlate with the severity of NASH. The observed associations in the FHS Gen 3 cohort were present in a cohort of individuals free of overt disease, and the effect size with hepatic steatosis was accordingly subtle. To verify the specificity and extend our observations, we next analyzed a hospital-based, case-control cohort that had more advanced and precisely phenotyped liver pathology. These patients consisted of obese individuals with biopsy-proven NASH (cases) compared with those with obesity and normal liver histology (controls). The clinical characteristics of the age-, sex-, and BMI-matched cohort are listed in Table 3, and the histologic characteris-

Table 2. Metabolite-phenotype associations in the Framingham Heart Study

	BMI		WC		Glucose		HOMA-IR	
	Est. β coefficient	*P* value	Est. β coefficient	*P* value	Est. β coefficient	*P* value	Est. β coefficient	*P* value
Uric acid	0.30	1.7E-18	0.29	1.9E-20	0.25	6.7E-14	0.25	6.6E-15
Glutamate	0.28	3.9E-18	0.28	1.1E-20			0.24	6.0E-16
Pyruvic acid	0.26	3.6E-17	0.25	1.1E-18	0.12	9.1E-05	0.21	7.8E-13
Quinolinic acid	0.23	1.1E-13	0.22	5.8E-15			0.19	2.3E-10
Anandamide	0.22	3.6E-13	0.20	1.6E-12	0.15	1.1E-06	0.15	2.1E-07
UDP-GlcNAc	0.27	2.4E-11	0.26	7.9E-11			0.25	4.0E-09
KIV	0.21	5.6E-11	0.18	5.1E-09	0.15	2.8E-06	0.15	1.1E-06
Glycine	−0.20	2.6E-10	−0.19	4.2E-11	−0.13	4.2E-05	−0.15	4.7E-07
Tyrosine	0.19	1.1E-09	0.17	1.1E-08			0.17	1.5E-08
Isoleucine	0.20	1.2E-09	0.18	1.0E-08	0.14	4.5E-05	0.16	3.7E-07
Valine	0.19	9.8E-09	0.16	7.1E-08			0.15	6.1E-07
Bilirubin	−0.17	2.7E-08	−0.18	1.1E-09				
2-Aminoadipic acid	0.25	7.0E-08	0.23	6.4E-07				
Hypoxanthine	0.17	8.9E-08	0.16	1.7E-08			0.14	1.4E-06
Kynurenine	0.18	9.0E-08	0.17	2.0E-08			0.17	5.5E-08
Oxalate	−0.16	1.3E-07	−0.14	2.7E-07				
Kynurenic acid	0.17	1.5E-07	0.16	1.8E-07			0.12	1.6E-04
Glucose	0.17	1.6E-07	0.16	1.4E-07	0.39	4.5E−34	0.19	5.3E-08
Aconitate	0.17	1.9E-07	0.17	1.3E-08	0.14	1.2E-05	0.18	4.8E-09
α-Ketoglutarate	0.16	2.3E-07	0.17	1.2E-08			0.20	7.8E-11
Xanthurenic acid	0.16	4.1E-07	0.15	1.1E-06			0.13	3.4E-05
Indole-3-propionic acid	−0.24	4.3E-07	−0.20	1.5E-06				
Leucine	0.16	1.6E-06	0.13	1.8E-05	0.13	2.1E-04	0.14	7.4E-06
C3-carnitine	0.15	3.0E-06	0.16	1.8E-08			0.13	3.3E-06
Alanine	0.14	6.8E-06	0.13	6.9E-06			0.12	4.7E-05
Glutathione reduced	−0.15	9.8E-06	−0.18	1.2E-08				
Proline	0.15	1.3E-05	0.13	3.7E-05				
Xanthine	0.14	2.0E-05	0.14	1.2E-05				
2-Hydroxybutyrate	0.13	3.5E-05						
Hippuric acid	−0.12	8.8E-05	−0.13	1.6E-05	−0.16	5.5E-07	−0.13	3.2E-05
Lactate	0.12	1.0E-04	0.11	5.8E-05				
Choline	0.12	1.4E-04					0.11	1.9E-04
Inosine	0.11	2.2E-04	0.11	1.2E-04				
C4-butyryl-carnitine							0.11	1.3E-04
C6-carnitine			0.15	1.0E-04				
KIC/KMV					0.12	2.1E-04		
Gluconate					0.20	4.3E-05		
Glycochenodeoxycholate							0.11	1.1E-04
Creatine							0.12	8.4E-05

WC, waist circumference; HOMA-IR, homeostatic model assessment of insulin resistance; Est., estimated; UDP-GlcNAc, uridine diphosphate *N*-acetylglucosamine; KIV, 2-ketoisovaleric acid; KIC, ketoisocaproic acid; KMV, ketomethylvaleric acid. Statistical values were obtained using age- and sex-adjusted regression.

tics of the liver biopsies are summarized in Supplemental Table 10. In univariate analysis, AEA was significantly higher in the NASH group compared with the control group (Table 3, $P < 0.002$). Multiple logistic regression demonstrated that AEA remained an independent predictor of NASH (OR 5.2, 95% CI 1.6-17.0, $P = 0.007$), after adjusting for known risk factors, including HDL, triglyceride level, HOMA-IR, and alanine aminotransferase (ALT) (Table 4). AEA was also associated with increased severity of NASH, as assessed by the NAFLD activity score (OR 4.8, 95% CI 1.6–13.8, $P = 0.005$) and the presence of fibrosis (22) (OR 2.6, 95% CI 1.01–6.5, $P = 0.04$; see Supplemental Table 10). These findings suggest that AEA is not only associated with biopsy-proven NASH, but also associated with advanced liver histopathology, and that it may serve as a biomarker for NASH.

Table 3. Characteristics of the NASH cohort

	Normal (*n* = 36)	NASH (*n* = 36)	*P* value
Age at biopsy (yr)	40.0 ± 9.7	43.1 ± 11.8	0.23
BMI, kg/m^2 (mean ± SD)	46.5 ± 7.0	47.9 ± 7.4	0.44
AST, U/l (median [range])	16.5 (0–61.0)	24.5 (13–179)	<0.0001
ALT, U/l (median [range])	27.0 (14.0–147.0)	48 (19–288)	<0.0001
Serum LDL, mg/dl (median [range])	89.7 (29.4–178.6)	91.6 (48.2–179.4)	0.92
Serum total cholesterol, mg/dl (median [range])	163 (80–260)	160 (101–276)	0.99
Serum triglycerides, mg/dl (median [range])	91 (44–266)	125 (39–418)	0.03
Serum HDL, mg/dl (median [range])	45 (25–105)	38.5 (25–73)	0.007
Fasting insulin, μU/ml (median [range])	20 (4–118)	32.5 (11–99)	0.002
Fasting glucose, mg/dl (median [range])	91 (65–224)	119.5 (74–263)	0.01
HOMA-IR (median [range])	4.8 (0.9–65.3)	8.6 (2.4–4 0.1)	0.001
Anandamide, pg/ml (mean ± SD)	104 ± 42	149 ± 72	0.002

NASH, nonalcoholic steatohepatitis; AST, aspartate aminotransferase; ALT, alanine aminotransferase; HOMA-IR, homeostatic model assessment of insulin resistance. Statistical values were obtained using Student's *t* or Mann-Whitney U test, depending on data normality.

Exogenous AEA alters glucose and lipid metabolism in zebrafish. To take the first preliminary steps toward ascertaining whether AEA may play a functional role in a model organism, we administered exogenous AEA to the zebrafish *Danio rerio*. We examined glucose and lipid metabolism, both of which were altered in our analyses of the FHS Gen 3 cohort. We conducted dose-response experiments in larval zebrafish that were exposed to increasing concentrations of AEA, which was added to the water to provide a constant reservoir of exogenous compound. Of note, several prior reports and our own preliminary studies showed that acute exogenous AEA administration in mice results in rapid metabolism, most likely by the fatty acid amide hydrolase, most likely by the fatty acid amide hydrolase, preventing the accumulation of AEA in blood and tissues (data not shown) (23, 24). When evaluating glucose homeostasis or lipid deposition, we found that administration of exogenous AEA was associated with increased glucose and lipid deposition (see Supplemental Methods). Furthermore, coadministration with the cannabinoid receptor inhibitor rimonabant ameliorated the AEA-induced elevation in glucose or lipid, underscoring the specificity of the observations (see Supplemental Methods).

Discussion

In this study, we developed a streamlined metabolomics method to investigate metabolites associated with cardiometabolic disease and NAFLD. Our analysis of a large, well-established, community-based cohort identified AEA as a candidate biomarker linking obesity and hepatic steatosis. Given the overall healthy status of the participants, the findings were subtle and represent associations many years before disease phenotypes develop. For this reason, we also studied AEA in a hospital-based, patient cohort with a histologically defined NAFLD together with carefully selected controls matched for age and BMI. Taken together, our study highlights the endocannabinoid system as a putative link among obesity, the metabolic syndrome, and liver pathology.

Our findings in relation to AEA are also in accord with prior studies of its cognate receptor. A role for the cannabinoid receptor CB1 in obesity and energy homeostasis has been established in relation to food intake and energy balance (25, 26). Activation of the CB1 receptor centrally and peripherally leads to altered energy balance and weight gain in model organisms (19, 27–29). Selective blockade of CB1 with rimonabant in human clinical trials demonstrated an effect on weight loss (30, 31), but further evaluation of cardiovascular outcomes was limited by psychiatric side effects, including an apparent increase in suicide risk (32). On the other hand, there is less data available on the direct role of AEA in metabolic disease. In accordance with our zebrafish data, rodents that are administered a high-fat diet demonstrate elevated AEA associated with weight gain and hyperglycemia (33, 34). However, the association of AEA with human obesity and glucose metabolism has been less certain (35–37) and has never been evaluated in a large human cohort free of overt disease — an important strength of the present study. The confirmation of our finding in two independent cohorts underscores the relevance of this pathway in human disease.

Table 4. Multivariable predictors for biopsy-proven NASH

	Odds ratio	95% Wald confidence limits		*P* value
Anandamide	5.20	1.48	20.05	0.007
ALT	1.05	1.01	1.08	0.01
HOMA-IR	1.01	0.95	1.07	0.88
HDL	0.92	0.85	0.99	0.03a
Triglycerides	1.01	0.997	1.02	0.16

NASH, nonalcoholic steatohepatitis; ALT, alanine aminotransferase; HOMA-IR, homeostatic model assessment of insulin resistance. Statistical values were obtained using multivariable logistic regression.

Our analysis also identified AEA as a candidate biomarker for NASH. Obesity and diabetes are risk factors that contribute to the increasing prevalence of hepatic steatosis and NAFLD in the US (2, 38). NASH can progress to cirrhosis or end-stage liver disease and is predicted to be the leading indication for liver transplantation by 2020 (39, 40). As only a subset of those with NAFLD progress to NASH and fibrosis, the ability to risk stratify patients and target only high-risk patients for liver biopsy is essential to limiting biopsy-related morbidity and mortality, while allowing for the accurate identification of high-risk patients (22). The finding that AEA level is associated with NASH severity, independent of traditional NASH risk factors, such as liver enzyme, HOMA-IR, HDL cholesterol, and lipid levels, suggests that this metabolite may serve as a biomarker of the presence and severity of NASH and may aid in elucidating the pathways that drive NASH progression. Although previous studies have implicated the endocannabinoid system in hepatic steatosis, either via altered regulation of the cannabinoid receptors (26) or in association with the related endocannabinoid 2-arachidonoylglycerol (21), our study is the first to our knowledge to implicate AEA specifically. The reasons for the closely related but not identical findings may be due to differences in the type of controls, matching of cases and controls, and differences in outcome measures. Future studies in a prospective cohort may help to clarify which endocannabinoid metabolites are associated with NAFLD and at which stage of severity this association begins.

Strengths of this analysis included a metabolite-profiling method with simplified preanalytical sample preparation, rapid separation, and optimized detection for human plasma metabolites. Maximizing the strengths of targeted methods, we developed a rapid approach that can routinely detect and quantify 179 analytes across key biologic pathways in human plasma. Our platform facilitates analysis in large cohorts, helping to overcome the risk for false-positive associations that can occur in multiple hypothesis testing (41). Whereas other studies have reported methods compatible with positive and negative polarity mass spectrometry (12, 42) or have developed multiplexing separation (43), our study represents both an improvement in the cycle time (~12.5 minutes) and a simplified preparation that facilitates metabolite quantification and replication in large patient cohorts.

Our study has limitations. Our biomarker analyses in the human cohorts identify associations and do not imply a causal relationship between AEA and NAFLD. Additional prospective cohort studies are needed to confirm our findings, adjust for potential confounders, and validate concentration thresholds for differentiating NASH from hepatic steatosis. Although our preliminary studies of exogenous administration of AEA in a vertebrate model demonstrated that excess AEA can lead to accumulation of lipid in the liver, additional work is needed to elucidate mechanisms and definitively demonstrate a causal relationship at more physiologically relevant levels. We also identified other candidate metabolites associated with cardiometabolic risk traits, including UDP-GlcNAc, hippuric acid, and reduced glutathione. It is possible that these biomarkers, which require further validation and study, may also predict liver disease, and future work is needed to determine the relative contributions of these other metabolites.

Taken together, our study supports the notion that metabolites such as AEA are fundamental biomarkers for metabolic disease, including obesity, insulin resistance, and NAFLD.

Methods

Subjects. The FHS Gen 3 cohort enrolled 4,095 individuals from 2002 to 2005 in a community-based longitudinal cohort study. Of 1,006 randomly selected participants, 1,000 were free of prevalent myocardial infarction or congestive heart failure at the first examination cycle and were selected for metabolite profiling.

Cardiometabolic traits, routine biochemical testing, and metabolite data were available for analysis in 997 of these subjects. 470 participants from FHS Gen 3 participants who had metabolite profiling also underwent an abdominal CT scan with evaluation for the presence of liver fat, as assessed by the liver-to-phantom ratio (44).

The Massachusetts General Hospital NAFLD cohort is a hospital-based cohort of individuals who have undergone clinically indicated liver biopsies and have available liver histology (2011–2016). The initial cohort contains a spectrum of NAFLD phenotypes, including normal liver histology, steatosis, NASH, and NASH with fibrosis. Individuals with other causes of chronic liver disease or with excess alcohol consumption, defined as >21 drinks per week for men and >14 drinks per week for women were excluded from this cohort (45). For the case-control study, patients with diabetes were excluded to remove the confounding effect of diabetes. Subjects with biopsy-proven NASH were matched by age, gender, and BMI to controls that exhibited normal liver histology. Liver biopsies were evaluated by a single blinded hepatopathologist and graded according to the NASH clinical research criteria for NAFLD activity score and fibrosis stage (22). NASH was defined by the presence at least of grade 1 steatosis, lobular inflammation, and hepatocyte ballooning. Normal liver histology had no evidence of steatosis, portal or lobular inflammation, hepatocyte ballooning, or fibrosis. Plasma samples used for analysis were drawn after a 12-hour fast within 3 months prior to liver biopsy.

Plasma samples. EDTA blood samples were collected and immediately centrifuged to separate cellular material from plasma. Aliquots of plasma were frozen on dry ice and stored at –80°C until analysis. 30-μl samples were deproteinized with 70 μl acetonitrile/methanol (75:25; v/v) containing deuterated internal standards (25 μM thymine-d_4 [Sigma-Aldrich], 10 μM inosine-$15N_4$ [Cambridge Isotope Laboratories], 10 μM citrulline-d_7 [Sigma-Aldrich], 25 μM phenylalanine-d_8 [Cambridge Isotope Laboratories], and 10 μM valine-d_8 [Sigma-Aldrich]). For some experiments in zebrafish lysates, AEA-d_4 [Cayman Chemical] was spiked into the matrix to generate the standard curve used to quantify AEA levels. After vortexing, the samples were centrifuged at 20,000 *g* at 4°C for 15 minutes, and supernatants were transferred to HPLC quality glass vials with inserts (MicroSolv). Additional sample preparation solvents that were evaluated (see Supplemental Methods) included acetonitrile/methanol/formic acid (75:25:0.1; v/v/v), acetonitrile/water/ammonium hydroxide (85:14:0.7), and methanol/water (80:20).

Chromatography. Deproteinized plasma extracts were subjected to normal phase hydrophilic interaction chromatography using a 2.1 × 100 mm 3.5-μm Xbridge amide column (Waters). Mobile phase A was 95:5 (v/v) water/acetonitrile, with 20 mM ammonium acetate and 20 mM ammonium hydroxide (pH 9.5). Mobile phase B was acetonitrile. Ammonium acetate, ammonium hydroxide, and Optima grade solvents were purchased from Fisher Scientific. For amide-negative mode, the chromatography system consisted of a 1260 Infinity autosampler (Agilent) connected to a 1290 Infinity HLPC binary pump system (Agilent). The initial conditions were 0.25 ml/min of 85% mobile phase B, followed by a linear gradient to 35% mobile phase B over 6 minutes. This was followed by a linear gradient to 2% mobile phase B over 0.5 minutes held for an additional 0.5 minutes and then a 0.5-minute gradient return to 85% mobile phase B. Column equilibration was continued for 4.5 minutes at 0.5 ml/min for a total cycle time of approximately 12.5 minutes. The column compartment was maintained at 30°C.

The chromatography for positive mode utilized an HTS PAL autosampler (Leap Technologies) connected to a 1260 HPLC binary system (Agilent). The same mobile phases and column were used as in the amide-negative mode, except that initial conditions were 0.25 ml/min of 90% mobile phase B. A linear gradient to 10% mobile phase B over 6 minutes was followed by a hold for 1 minute at 10% mobile phase B. The initial conditions were restored over 0.5 minutes, and the column was equilibrated for 4.5 minutes at 0.5 ml/min. Although these methods were developed in parallel on separate LC-MS/MS instruments, the method can be run routinely on a single instrument, alternating a sample injection in the positive and then negative modes.

Mass spectrometry. Using purified reference standards, 157 metabolites were optimized for negative-mode detection on a 6490 QQQ (Agilent) triple-quadrupole mass spectrometer equipped with an electrospray ionization source. Transitions for each compound were assessed for sensitivity, selectivity, and retention time in the pooled plasma matrix with and without the spiked reference standard. 78 of the metabolites were reproducibly detected in human plasma and were selected for dynamic multiple reaction monitoring (MRM), which had a minimum dwell time of 30 milliseconds for each metabolite. Final mass spectrometry settings for the 6490 QQQ were as follows: sheath gas temperature, 400°C; sheath gas flow, 12 l/min; drying gas temperature, 290°C; drying gas flow, 15 l/min; capillary, 4,000 V; nozzle pressure, 30 psi; nozzle voltage, 500 V; and delta EMV, 200 V.

A similar strategy was used to generate a positive ionization mode MRM method, except that a QTrap 4000 (Applied Biosystems/Sciex) mass spectrometer was used. Of 114 metabolites optimized for positive mode, 101 were detectable in human plasma and included in the final MRM method. The final mass spectrometry settings for the QTrap 4000 were as follows: source temperature, 450°C; ion spray voltage, 5,000 V; CAD gas, 10; CUR gas, 20.

Peak integration, normalization, and quality control. Metabolite quantification was determined by integrating peak areas using MassHunter QQQ Quant (Agilent) or Multiquant software (version 2.0; Applied Biosystem/Sciex). All metabolite peaks were manually reviewed for peak quality in a blinded manner. In addition, pooled plasma samples were interspersed within each analytical run at standardized intervals every 10 injections, enabling the monitoring and correction for temporal drift in mass spectrometry performance (46). Each of these samples was prepared, extracted, and processed from a larger pool of normal human plasma. The nearest neighbor flanking pair of pooled plasma was used to normalize experimental samples in a metabolite-by-metabolite manner. In addition, a separate pooled plasma sample was included every 20 injections to assess the performance of the normalization procedure and determine the coefficient of variation (CV) for each metabolite. The CV of each analyte is included in Supplemental Table 1. Any sample with deuterated internal standard values ≥2 SD was excluded from peak integration and further analysis. Validation of peak identity of AEA is shown in the Supplemental Methods.

Statistics. All metabolite values were natural logarithmically transformed because of their nonnormal distribution and then standardized (to mean = 0, SD = 1) within the cohort. Age- and sex-adjusted regression analyses were performed in each study sample to examine the relation of each metabolite (predictor variable) to each clinical metabolic trait (response variables): BMI, fasting glucose, log HOMA-IR, systolic blood pressure, diastolic blood pressure, log triglycerides, and HDL cholesterol. Linear regression analyses were performed with adjustment for age, sex, and batch on the LC-MS run (see Supplemental Tables 2–9). Given that 179 metabolites were analyzed across both methods, we used a Bonferroni-corrected P value threshold of 2.79×10^{-4} to account for the number of metabolites analyzed. Because the majority of metabolites were correlated within well-defined biological groups (amino acids, nucleotides, Krebs cycle organic acids, etc.), this correction was conservative.

Clinical and laboratory continuous variables were compared between two independent groups using 2 tailed Student's t test or Mann-Whitney test, as appropriate. Categorical variables were compared using Fisher's exact test. For the metabolite analysis in the animal samples, we used a P value threshold of 0.05, using Mann-Whitney or Student's t test, depending on data normality. Statistical analyses were performed using SAS (SAS Institute) (see Supplemental Figures).

Study approval. All human study protocols were approved by the institutional review board (Massachusetts General Hospital), and all study participants provided written informed consent.

Author contributions

WTK and REG designed the study; WTK, JO, and AKN performed experiments; MTL, RV, TJW, and KEC provided data and samples; MK, QY, and MGL conducted statistical analysis; WTK, MK, QY, MGL, RTP, and REG analyzed data; and WTK, AKN, KEC, and REG wrote the manuscript, XS contributed to performing the experiments and reviewing and revising the manuscript for critical content. All authors reviewed and revised the manuscript for critical content.

Acknowledgments

This study was supported by NIH grant K23NS076597 and R01NS099209 (to WTK), American Heart Association grant 14GRNT19060044 (to WTK), NIH grant K23DK99422 (to KEC), and NIH grants R01HL098280, U01DK048489, and R01DK081572 (to REG).

Address correspondence to: Robert E. Gerszten, Division of Cardiovascular Medicine, Beth Israel Deaconess Medical Center, 330 Brookline Avenue, Boston, Massachusetts 02115, USA. Phone: 617.632.7647; E-mail: rgerszte@bidmc.harvard.edu.

1. Marchesini G, et al. Nonalcoholic fatty liver, steatohepatitis, and the metabolic syndrome. *Hepatology*. 2003;37 (4):917–923.
2. Fabbrini E, Sullivan S, Klein S. Obesity and nonalcoholic fatty liver disease: biochemical, metabolic, and clinical implications. *Hepatology*. 2010;51 (2):679–689.
3. Yki-Järvinen H. Non-alcoholic fatty liver disease as a cause and a consequence of metabolic syndrome. *Lancet Diabetes Endocrinol*. 2014;2 (11):901–910.
4. Sinn DH, et al. Persistent nonalcoholic fatty liver disease increases risk for carotid atherosclerosis. *Gastroenterology*. 2016;151(3):481–488.e1.
5. Ma J, et al. Bi-directional analysis between fatty liver and cardiovascular disease risk factors. *J Hepatol*. 2017;66 (2):390–397.
6. Suhre K, et al. Human metabolic individuality in biomedical and pharmaceutical research. *Nature*. 2011;477(7362):54–60.
7. Floegel A, et al. Identification of serum metabolites associated with risk of type 2 diabetes using a targeted metabolomic approach. *Diabetes*. 2013;62 (2):639–648.
8. Wang-Sattler R, et al. Novel biomarkers for pre-diabetes identified by metabolomics. *Mol Syst Biol*. 2012;8:615.
9. Würtz P, et al. Metabolite profiling and cardiovascular event risk: a prospective study of 3 population-based cohorts. *Circulation*. 2015;131 (9):774–785.
10. Würtz P, et al. Branched-chain and aromatic amino acids are predictors of insulin resistance in young adults. *Diabetes Care*. 2013;36 (3):648–655.
11. Wang TJ, et al. Metabolite profiles and the risk of developing diabetes. *Nat Med*. 2011;17 (4):448–453.
12. Yuan M, Breitkopf SB, Yang X, Asara JM. A positive/negative ion-switching, targeted mass spectrometry-based metabolomics platform for bodily fluids, cells, and fresh and fixed tissue. *Nat Protoc*. 2012;7 (5):872–881.
13. Fenn JB, Mann M, Meng CK, Wong SF, Whitehouse CM. Electrospray ionization for mass spectrometry of large biomolecules. *Science*. 1989;246(4926):64–71.
14. Facchini F, Chen YD, Hollenbeck CB, Reaven GM. Relationship between resistance to insulin-mediated glucose uptake, urinary uric acid clearance, and plasma uric acid concentration. *JAMA*. 1991;266 (21):3008–3011.
15. Wang TJ, et al. 2-Aminoadipic acid is a biomarker for diabetes risk. *J Clin Invest*. 2013;123 (10):4309–4317.
16. Cheng S, et al. Metabolite profiling identifies pathways associated with metabolic risk in humans. *Circulation*. 2012;125 (18):2222–2231.
17. Wang TJ, et al. Metabolite profiles and the risk of developing diabetes. *Nat Med*. 2011;17 (4):448–453.
18. Newgard CB, et al. A branched-chain amino acid-related metabolic signature that differentiates obese and lean humans and contributes to insulin resistance. *Cell Metab*. 2009;9 (4):311–326.
19. Osei-Hyiaman D, et al. Endocannabinoid activation at hepatic CB1 receptors stimulates fatty acid synthesis and contributes to diet-induced obesity. *J Clin Invest*. 2005;115 (5):1298–1305.
20. Tam J, et al. Peripheral CB1 cannabinoid receptor blockade improves cardiometabolic risk in mouse models of obesity. *J Clin Invest*. 2010;120 (8):2953–2966.
21. Zelber-Sagi S, et al. Serum levels of endocannabinoids are independently associated with nonalcoholic fatty liver disease. *Obesity (Silver Spring)*. 2017;25 (1):94–101.
22. Kleiner DE, et al. Design and validation of a histological scoring system for nonalcoholic fatty liver disease. *Hepatology*. 2005;41 (6):1313–1321.
23. Willoughby KA, Moore SF, Martin BR, Ellis EF. The biodisposition and metabolism of anandamide in mice. *J Pharmacol Exp Ther*. 1997;282 (1):243–247.
24. Smith PB, Compton DR, Welch SP, Razdan RK, Mechoulam R, Martin BR. The pharmacological activity of anandamide, a putative endogenous cannabinoid, in mice. *J Pharmacol Exp Ther*. 1994;270 (1):219–227.
25. Di Marzo V, et al. Leptin-regulated endocannabinoids are involved in maintaining food intake. *Nature*. 2001;410 (6830):822–825.
26. Silvestri C, Di Marzo V. The endocannabinoid system in energy homeostasis and the etiopathology of metabolic disorders. *Cell Metab*. 2013;17 (4):475–490.
27. Cota D, et al. The endogenous cannabinoid system affects energy balance via central orexigenic drive and peripheral lipogenesis. *J Clin Invest*. 2003;112 (3):423–431.
28. Pai WY, Hsu CC, Lai CY, Chang TZ, Tsai YL, Her GM. Cannabinoid receptor 1 promotes hepatic lipid accumulation and lipotoxicity through the induction of SREBP-1c expression in zebrafish. *Transgenic Res*. 2013;22 (4):823–838.
29. Fraher D, et al. Lipid Abundance in Zebrafish Embryos Is Regulated by Complementary Actions of the Endocannabinoid System and Retinoic Acid Pathway. *Endocrinology*. 2015;156 (10):3596–3609.
30. Pi-Sunyer FX, Aronne LJ, Heshmati HM, Devin J, Rosenstock J, RIO-North America Study Group. Effect of rimonabant, a cannabinoid-1 receptor blocker, on weight and cardiometabolic risk factors in overweight or obese patients: RIO-North America: a randomized controlled trial. *JAMA*. 2006;295(7):761–775.
31. Després JP, Golay A, Sjöström L, Rimonabant in Obesity-Lipids Study Group. Effects of rimonabant on metabolic risk factors in overweight patients with dyslipidemia. *N Engl J Med*. 2005;353 (20):2121–2134.
32. Topol EJ, et al. Rimonabant for prevention of cardiovascular events (CRESCENDO): a randomised, multicentre, placebo-controlled trial. *Lancet*. 2010;376 (9740):517–523.
33. Matias I, Petrosino S, Racioppi A, Capasso R, Izzo AA, Di Marzo V. Dysregulation of peripheral endocannabinoid levels in hyperglycemia and obesity: Effect of high fat diets. *Mol Cell Endocrinol*. 2008;286 (1-2 Suppl 1):S66–S78.
34. Izzo AA, et al. Peripheral endocannabinoid dysregulation in obesity: relation to intestinal motility and energy processing induced by food deprivation and re-feeding. *Br J Pharmacol*. 2009;158 (2):451–461.
35. Blüher M, et al. Dysregulation of the peripheral and adipose tissue endocannabinoid system in human abdominal obesity. *Diabetes*. 2006;55 (11):3053–3060.
36. Di Marzo V, et al. Changes in plasma endocannabinoid levels in viscerally obese men following a 1 year lifestyle modification programme and waist circumference reduction: associations with changes in metabolic risk factors. *Diabetologia*. 2009;52 (2):213–217.
37. Matias I, et al. Regulation, function, and dysregulation of endocannabinoids in models of adipose and beta-pancreatic cells and in obesity and hyperglycemia. *J Clin Endocrinol Metab*. 2006;91 (8):3171–3180.

38. Tiniakos DG, Vos MB, Brunt EM. Nonalcoholic fatty liver disease: pathology and pathogenesis. *Annu Rev Pathol*. 2010;5:145–171.
39. Harrison SA, Neuschwander-Tetri BA. Nonalcoholic fatty liver disease and nonalcoholic steatohepatitis. *Clin Liver Dis*. 2004;8(4):861–879.
40. Bhala N, et al. The natural history of nonalcoholic fatty liver disease with advanced fibrosis or cirrhosis: an international collaborative study. *Hepatology*. 2011;54(4):1208–1216.
41. Broadhurst D, Kell DB. Statistical strategies for avoiding false discoveries in metabolomics and related experiments. *Metabolomics*. 2006;2:171–196.
42. Bajad SU, Lu W, Kimball EH, Yuan J, Peterson C, Rabinowitz JD. Separation and quantitation of water soluble cellular metabolites by hydrophilic interaction chromatography-tandem mass spectrometry. *J Chromatogr A*. 2006;1125 (1):76–88.
43. Wei R, Li G, Seymour AB. High-throughput and multiplexed LC/MS/MRM method for targeted metabolomics. *Anal Chem*. 2010;82 (13):5527–5533.
44. Speliotes EK, et al. Liver fat is reproducibly measured using computed tomography in the Framingham Heart Study. *J Gastroenterol Hepatol*. 2008;23 (6):894–899.
45. Chalasani N, et al. The diagnosis and management of non-alcoholic fatty liver disease: practice Guideline by the American Association for the Study of Liver Diseases, American College of Gastroenterology, and the American Gastroenterological Association. *Hepatology*. 2012;55(6):2005–2023.
46. Dunn WB, et al. Procedures for large-scale metabolic profiling of serum and plasma using gas chromatography and liquid chromatography coupled to mass spectrometry. *Nat Protoc*. 2011;6 (7):1060–1083.

Supplemental Data

Metabolite Profiling Identifies Anandamide as a Biomarker of Nonalcoholic Steatohepatitis

W. Taylor Kimberly, MD, PhD,[1] John O'Sullivan, MD, PhD,[2] Anjali K. Nath, PhD,[3] Michelle Keyes, PhD,[4] Xu Shi, PhD,[2] Martin G. Larson, SD,[4,5] Qiong Yang, PhD,[4,5] Michelle T. Long, MD,[4,6] Ramachandran Vasan, MD,[4] Randall T. Peterson, PhD,[3] Thomas J. Wang, MD,[7] Kathleen E. Corey, MD, MPH, MMSc[8] and Robert E. Gerszten, MD[2]

1. Center for Human Genetic Research, Department of Neurology, Massachusetts General Hospital, Boston, MA
2. Division of Cardiovascular Medicine, Beth Israel Deaconess Hospital, Boston, MA
3. Division of Cardiology, Department of Medicine, Massachusetts General Hospital, Boston, MA
4. Framingham Heart Study of the National Heart, Lung, and Blood Institute and Boston University School of Medicine, Framingham, MA
5. Biostatistics Department, Boston University School of Public Health, Boston, MA
6. Section of Gastroenterology, Department of Medicine, Boston University School of Medicine, Boston, MA
7. Division of Cardiovascular Medicine, Department of Medicine, Vanderbilt University, Nashville, TN
8. Division of Gastroenterology, Department of Medicine, Massachusetts General Hospital, Boston, MA

Correspondence:
Robert E. Gerszten, MD
Division of Cardiovascular Medicine
Beth Israel Deaconess Medical Center
330 Brookline Ave
Boston, MA 02115
Email: rgerszte@bidmc.harvard.edu

Supplemental Methods and Results

Analyte selection

In order to develop a multifunctional, high throughput method for human plasma that included sentinel analytes across important metabolic pathways, we first identified 273 metabolites available in purity across major domains of metabolism in the KEGG database. Analytes included central carbohydrates, organic acids, bile acids, sterols, glycans, nucleotides, vitamins, and amino acids. Next, we constrained the design based on the following principles: 1) compatibility with a one-step pre-analytical sample preparation, 2) a rapid LC gradient with sufficient separation of metabolites to allow for multiple reaction monitoring, 3) stable retention times and column life over repeated injections, and 4) optimization of mass spectrometer settings to enhance detection of lower abundance negatively charged metabolites. The conceptual workflow of the LC-MS/MS method is depicted in Supplemental Figure 1. Each metabolite was individually tuned on the platform. The example of 2-aminoadipic acid (2-AAA) demonstrates the identity and separation from isobaric contaminants (Supplemental Fig. 1B). Detection of the endogenous metabolite in plasma was compared to exogenous compound in a pure preparation and exogenous compound spiked into plasma to confirm identity. The expected peak was further identified by examining fragmentation patterns and comparing to pure exogenous compound.

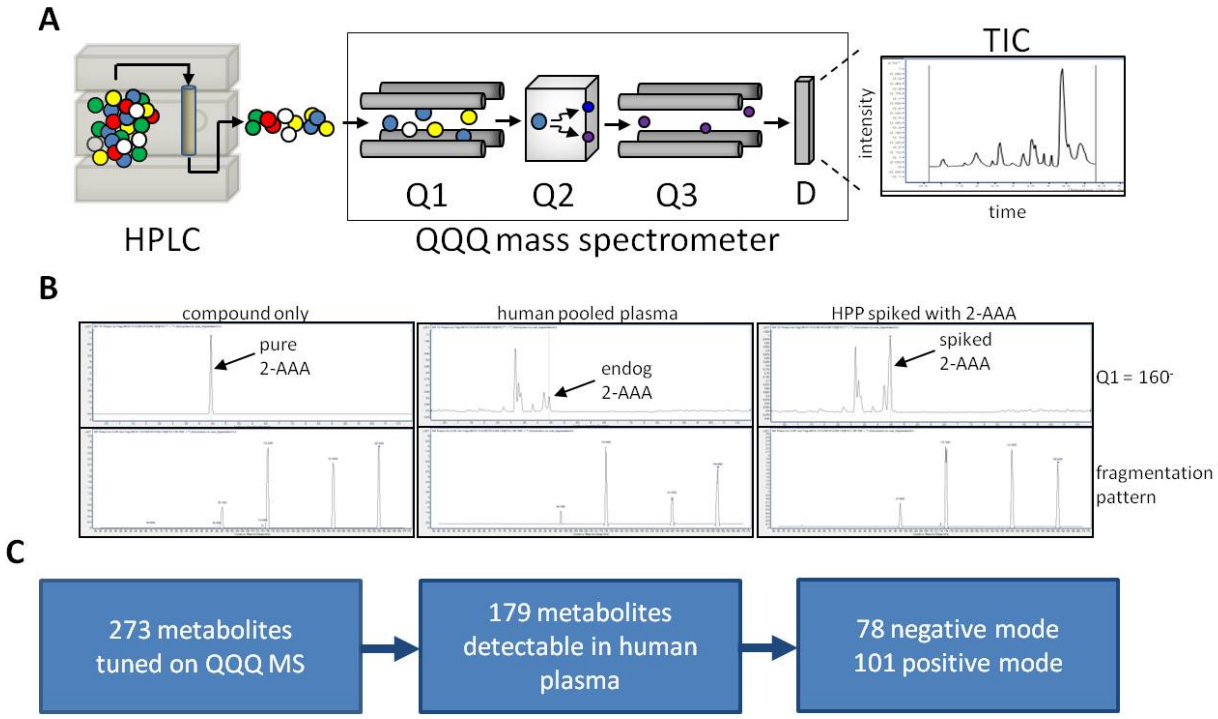

Supplemental Figure 1. Conceptual workflow for metabolite profiling. A) Following precipitation of protein, the complex matrix is first separated using Amide chromatography followed by tandem mass spectrometry to identify each metabolite. **B)** The process for compound identification first involves tuning the instrument to purified compound (left panels). Human pooled plasma is then monitored using the optimized settings (middle panel). Isobaric contaminants demonstrate different retention times and peak identity is further confirmed by comparing fragmentation patterns with the pure compound. Finally, spiked compound is added to the pooled plasma to confirm proper retention time. **C)** Overview of the number of initial compounds tuned on the platform, the number that were detectable in human plasma (middle panel) and the number based on ionization polarity.

Platform settings influence sensitivity in a compound-specific manner

We assessed for analytical parameters that affect sensitivity and reproducibility. We focused on sensitivity first, to maximize the number of monitored analytes detected in a high throughput method. The sensitivity to various metabolite classes was dependent upon source ionization and sample preparation conditions, which influenced detection in a compound-specific manner (see Supplemental Figure 2). For example, altering the desolvation rate by increasing source gas temperatures improved the sensitivity for many compound classes but particularly for nucleotides, high energy phosphates and bile acids (Supplemental Figure 2A). Other source settings related to the electrospray pressure and nozzle voltage demonstrated a trade-off in sensitivity for different metabolite classes (Supplemental Figure 2B). Similarly, the sample preparation solvents influenced both the sensitivity and the ability to detect selected compounds, with acetonitrile:methanol preserving the maximum detection of metabolites with the highest sensitivity (Supplemental Figure 2C). Of 273 compounds evaluated, the final method yielded 179 metabolites that were reproducibly detected in human plasma.

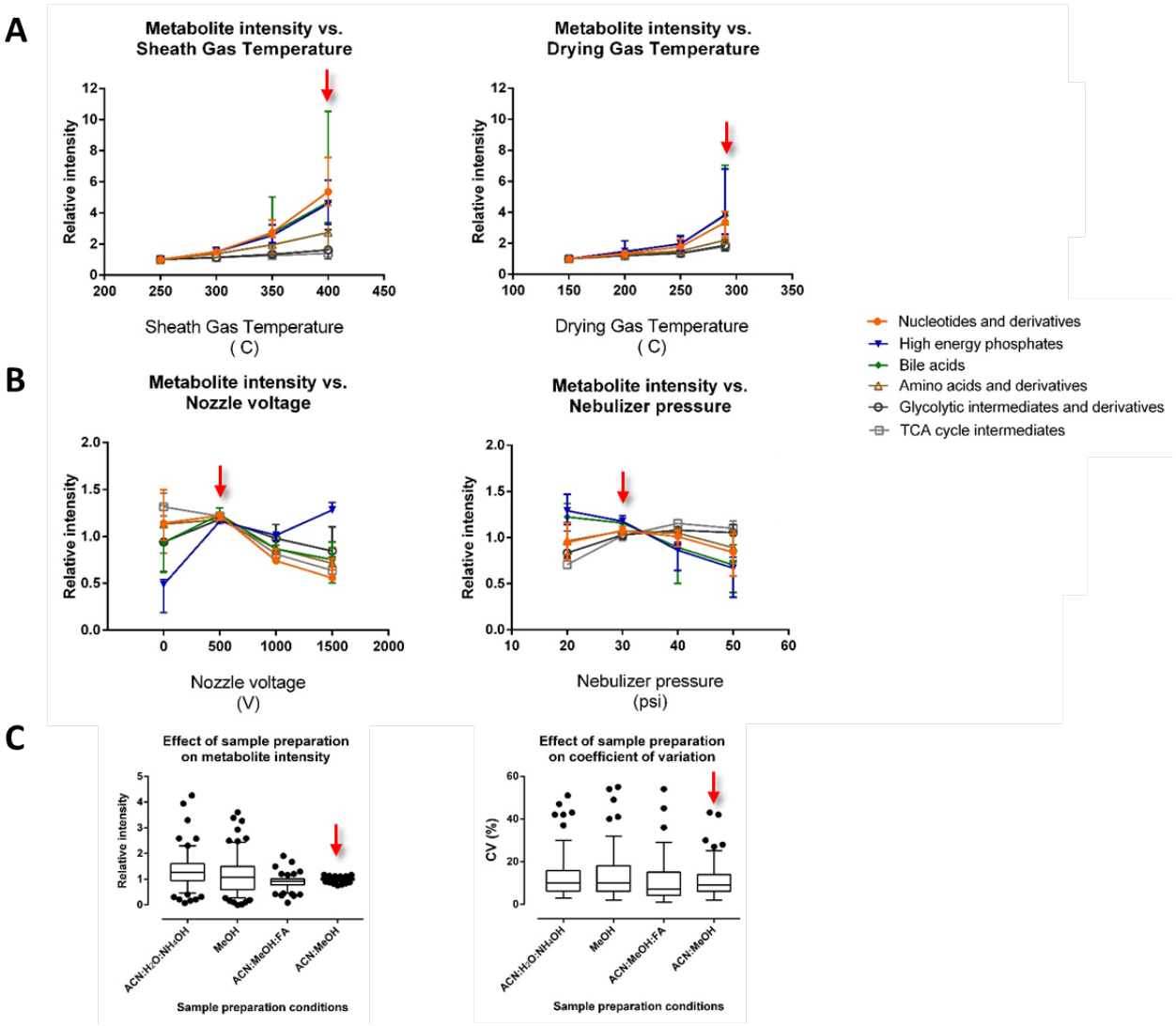

Supplemental Figure 2. Sensitivity for detection varies in a compound-specific manner. A) Ionization source settings that impact the desolvation rate, including the sheath and drying gas temperatures affect sensitivity that varies by compound class. The arrow marks the final setting used for subsequent analysis. **B)** Source voltage and nebulizer pressures demonstrate a trade-off in the detection of compound classes, with the optimal setting highlighted by the red arrows. **C)** Sample preparation solvents altered the sensitivity for detection of compounds, and to a lesser extent, the coefficient of variation (CV).

Analysis of retention time, normalization procedures and reproducibility

We conducted a test run composed of 700 sample injections to evaluate retention time (RT) and reproducibility of the normalization procedure. Evaluating the RTs for all analytes demonstrated that temporal drift remained within a ~5 second window throughout the run (Supplemental Figure 3A). In order to evaluate analytical reproducibility, we first corrected for the effect of ionization suppression, a consequence of electrospray ionization related to the accumulation of salts and sample biomass in the ionization source that can lead to sensitivity drift over time (Supplemental Figure 3B).[1] Interspersed pooled plasma reference samples allowed for correction of the anticipated sensitivity drift (Supplemental Figure 3C), resulting in coefficient of variation (CV) of 4.3% to 11.9% for the deuterated internal standards (Supplemental Figure 3D). Measurement variation was also specific to each analyte[2] in the pooled plasma reference samples, with CV ranging from 1.0% to 22.1% (see Supplemental Table 1).

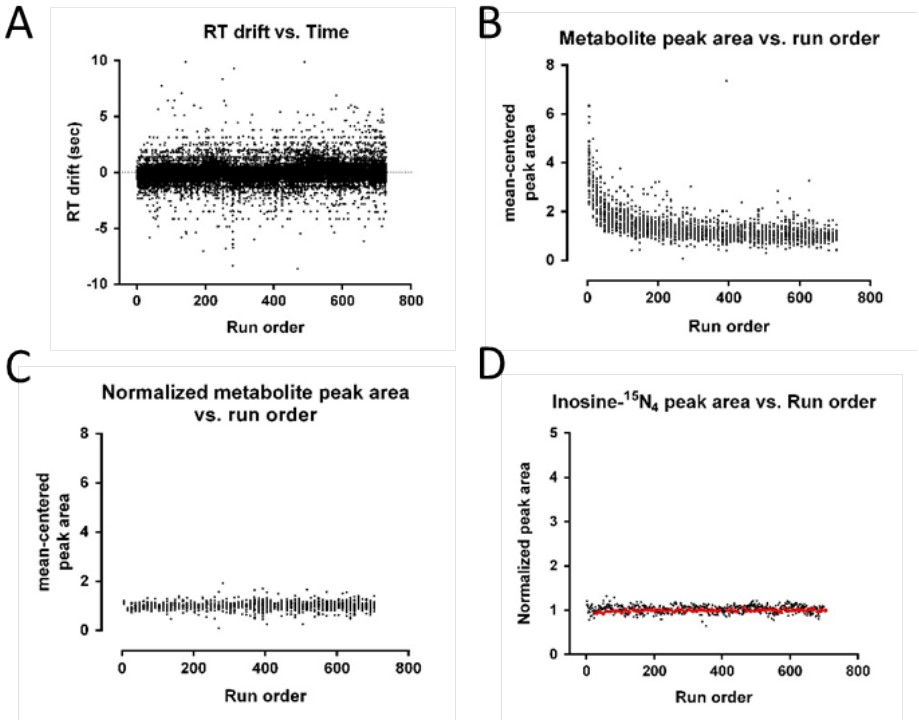

Supplemental Figure 3. Assessment of reproducibility and validation of the pooled plasma normalization procedure. A) The retention time (RT) drift over a 700 sample injection run is plotted for all metabolites on a sample by sample basis. With a multiple reaction monitoring window of 30-60 seconds per metabolite allows for the observed drift in retention time over long runs. **B)** Ionization suppression is evident in negative mode Amide LC-MS/MS, which is related to the accumulation of salts and biomass that occurs with repeated injections. **C)** Normalization on a metabolite-by-metabolite basis corrects sensitivity drift. Data for interspersed human pooled plasma samples are shown. **D)** Deuterated internal standards are included in every sample to visualize and confirm expected sensitivity and normalization. Inosine-$^{15}N_4$ is shown as an example, which had a CV of 5.6% across all injections.

The biological range of values for each metabolite within the experimental samples varied to a greater extent than analytical variation, although some metabolites demonstrated less variation suggestive of tighter regulation (e.g., citrulline, Supplemental Figure 4A). Other analytes demonstrated wider variation in concentration in the experimental samples (e.g., the ketone body 3-hydroxybutyrate, Supplemental Figure 4B), suggestive of a greater tolerance in concentration range within the bloodstream. For each metabolite, the relationship between the analytical and biological variation (Supplemental Figure 4C) was determined by the interaction between platform analytical performance and the biological concentration range in the plasma. For some compound classes such as the ketone bodies and bile acids, there was approximately a five-fold greater biological to analytical variation whereas the TCA cycle organic acids demonstrated less dynamic range (Supplemental Figure 4C, red versus green dots, respectively).

To assess suitability for population based studies, we developed clinical sample size estimates which varied depending on the analytical variation for each metabolite and the biological variation of the analyte within the experimental samples (i.e., the difference between the means). Generalizing this concept, we modeled this relationship based on sample size for group size *N*, the difference between the means (as a percentage) and the CV at 80% power, using a Bonferroni-corrected type I error rate for 179 tests, $\alpha=2.79\times10^{-4}$.[3] Sample size calculations were modeled for different coefficient of variation thresholds based on the equation:

$$n = \frac{(z_{1-\alpha/2} + z_{1-\beta})^2 \, CV^2 \, (f^2+1)}{(f-1)^2}$$

where n is the number of observations per group, z is the z score for the standard normal distribution, f is the ratio of the means between each group, Type I error is set at $\alpha=2.79\times10^{-4}$ and the power is set at $1-\beta=0.80$.[3]

Given the observed analytical variability up to 22.1%, a cohort of 1,000 subjects would have 80% power to detect a difference of 8% or less for all metabolites included in the platform (Supplemental Figure 4D), which corresponds to a magnitude commonly seen in metabolite profiling studies.[4-7]

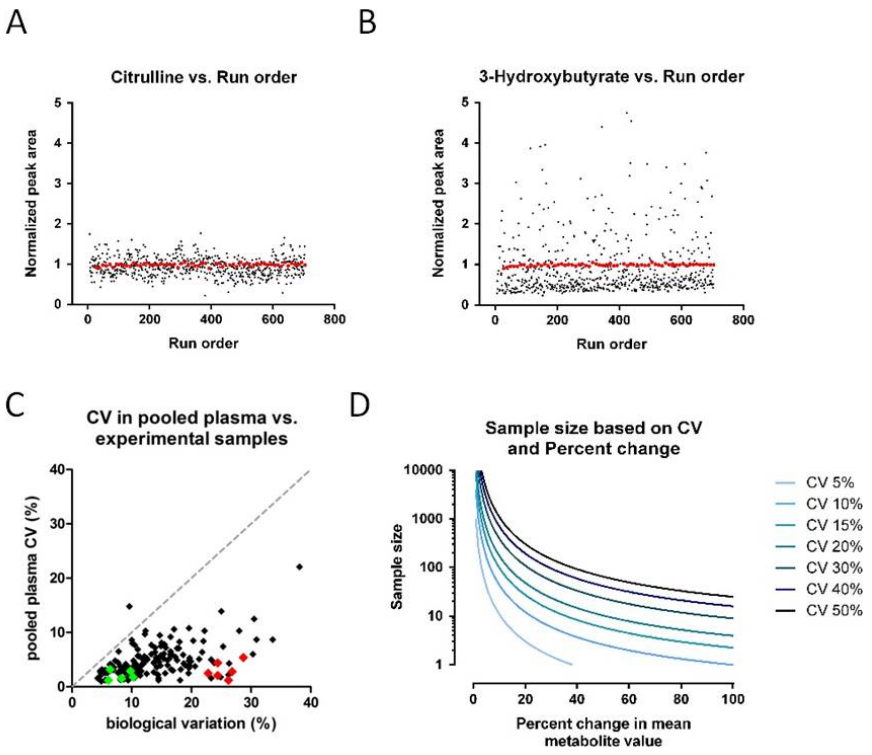

Supplemental Figure 4. Both analytical and biological factors are analyte specific and determine the power in a given sample size. **A)** On a metabolite-by-metabolite basis, the reproducibility of detection was monitored throughout the analytical run by interspersing human pooled plasma replicates (red dots). The experimental samples (black dots) are representative of the biological variability of the metabolite. Citrulline demonstrated less biological variability relative to **B)** the ketone body, 3-hydroxybutyrate. **C)** Summary of the analytical coefficient of variation (CV) in pooled plasma replicates relative to the biological variation of the experimental samples. As illustrative examples, ketone bodies and bile acids (red dots) demonstrated greater biological variation than tricarboxylic organic acids (green dots). **D)** Sample size estimates are modeled based on a given analytical CV (each line represents a different CV threshold), the percentage difference in values between cases and controls. For these models, 80% power and a Bonferroni-corrected type I error rate for 179 tests, $\alpha=2.79\times10^{-4}$ was used.

Peak validation of anandamide

Each metabolite was individually tuned on the platform. Detection of the endogenous metabolite in plasma was compared to exogenous compound in a pure preparation and exogenous compound spiked into plasma to confirm identity. Supplemental Figure 5 shows the chromatograms from anandamide (AEA), which demonstrate the unambiguous identity of pure exogenous anandamide injected onto the LC-MS system (Supplemental Fig. 5A), which also corresponds to the same peak when exogenous AEA was spiked into human plasma (Supplemental Fig. 5B). The endogenous AEA in human plasma (Supplemental Fig. 5C) was detected and showed no isobaric contaminants. Both high and low endogenous AEA (Supplemental Fig. 5D) from experimental samples are shown.

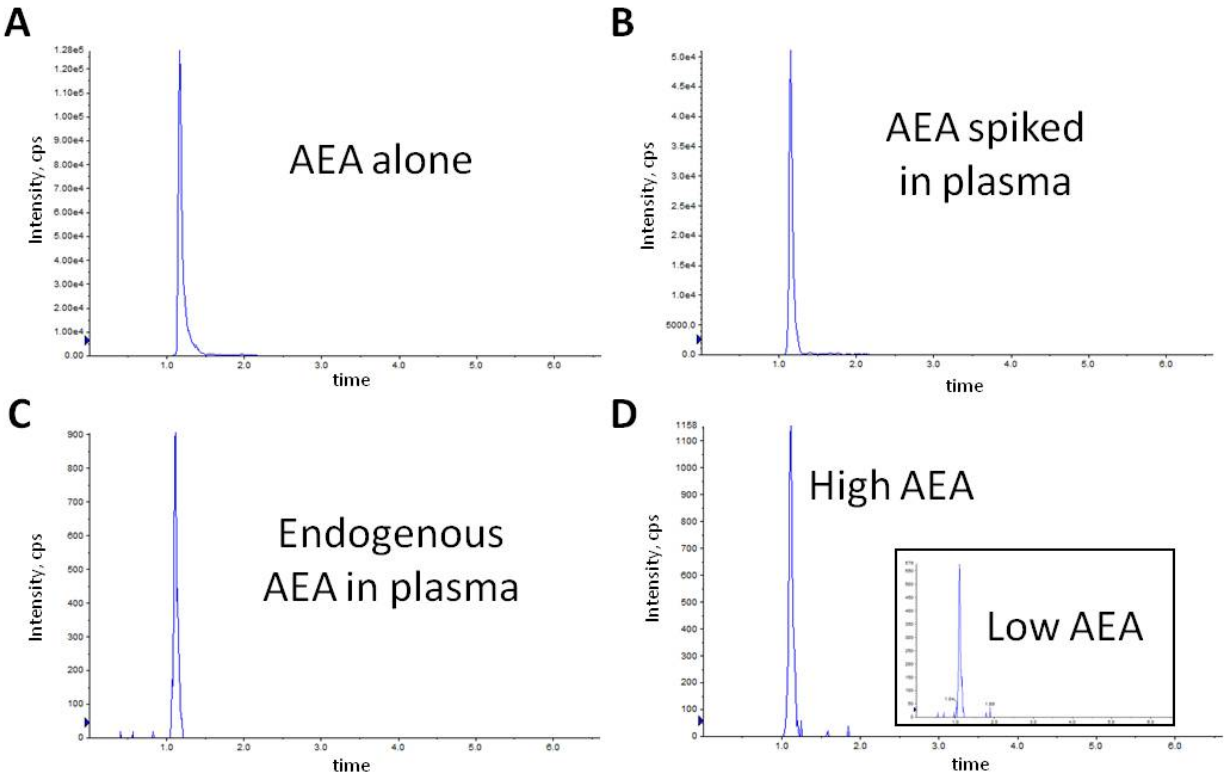

Supplemental Figure 5. Validation and peak identity of anandamide in the Amide LC-MS method. A) Exogenous anandamide (AEA) was injected into the LC-MS using the Amide method. The AEA peak, with MRM transitions of Q1: 348, Q3: 62.3, is shown in panel A. **B)** Anandamide was also spiked into normal volunteer human plasma, and the same peak was

identified. **C)** The endogenous level of anandamide was detected at the same retention time, and no contaminating peaks were detected elsewhere in the run with same MRM settings. **D)** Two examples of experimental samples from the Framingham Heart Study Generation 3 cohort, with high endogenous anandamide (larger panel) and low endogenous anandamide (inset). Note that the low AEA chromatogram is scaled to match the high AEA peak intensity so that the peak and area of each peak can be directly compared.

Anandamide concentration in plasma

To estimate the absolute concentration of anandamide in plasma, exogenous deuterated anandamide-d_4 was spiked into human pooled plasma across a broad concentration range. Supplemental Figure 6 shows the wide linear range (right hand panel) as well as the range that corresponds to the concentration of endogenous anandamide (left hand panel). The calculated concentration in human pooled plasma was 106 ± 5.7 pg/ml.

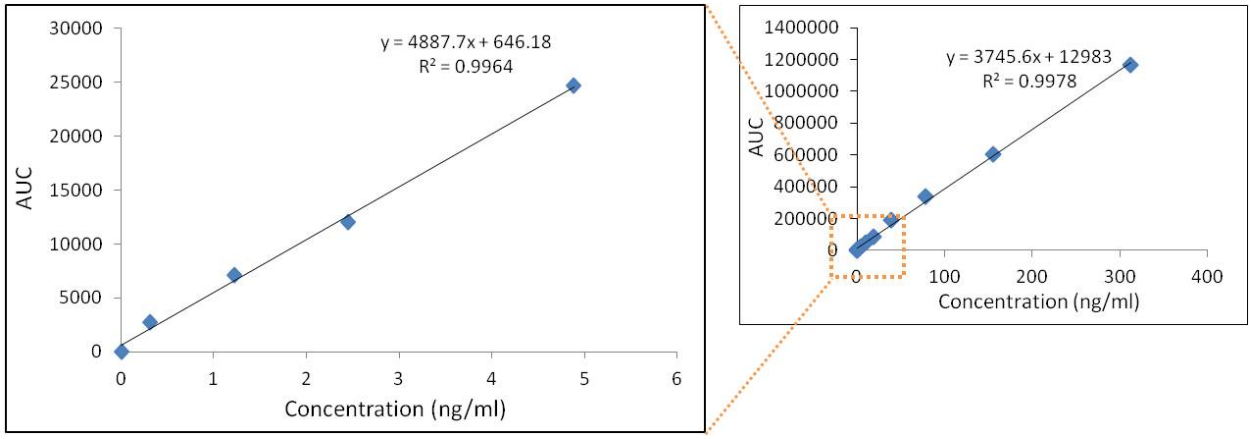

Supplemental Figure 6. Standard curve demonstrating the range of detection of anandamide-d_4 in human plasma. A) Isotopically labeled anandamide-d_4, was spiked into human plasma at the indicated concentrations and analyzed using the LC-MS amide protocol. The lefthand panel is an inset that corresponds to the organge dotted rectangle on the righthand panel. Based on the standard curve, endogenous anandamide in normal volunteer plasma was measured at 106 ± 5.7 pg/ml, which is consistent with published concentration ranges.

***D. rerio* experiments**

Zebrafish (Ekkwill strain) were maintained and embryos were obtained according to standard fish husbandry protocols in accordance with the Massachusetts General Hospital Institutional Animal Care and Use Committee. All compounds were purchased from Sigma-Aldrich. Compounds were incubated for the indicated times, and the concentration indicates the level in the water. The corresponding level within the fish varies based on absorption through the skin, metabolism and excretion. However, the level of anandamide obtained within the zebrafish, as measured by mass spectrometry, exceeded the endogenous level in order to demonstrate an effect of administration even if greater than physiological normal levels. Post treatment, viability of the zebrafish larvae was assessed by observing heart rate and sedation was assessed by the touch response reflex. Glucose concentration was measured using Amplex Red Glucose Assay Kit (Invitrogen) and converted to uM concentration using a standard curve, according to the manufacturer's instructions. Product formation was determined by reading fluorescence emission at 595nm. Lipid deposition was assessed using Oil Red O staining. Zebrafish were fixed in 4% paraformaldehyde, stained with 0.3% Oil Red O in propylene glycol, washed with propylene glycol and imaged in 80% glycerol. Triglycerides were measured in whole zebrafish larvae by homogenizing 20 fish in 50 µl of water. The lysate was centrifuged at 6000 RPM for 10 minutes at 4°C and the supernatant was used to assess triglyceride levels using the Cayman Chemical kit according to the manufacturer's instructions.

Accumulation of AEA within the fish embryos was confirmed by comparison to anandamide-d_4 internal standard two hours after addition of 30 µM AEA to the water (Figure 7A). To determine the effect of acute administration of AEA on glucose homeostasis, zebrafish larvae 6 days post fertilization (dpf) were supplemented with AEA. One hour post

administration, larvae displayed elevated glucose levels (10,067±345 RFU vs 7,653±312 RFU, p=0.0001; Figure 7B, left panel). At the highest concentration (30 μM AEA), there was a 32% elevation in glucose at 1 hour, a 43% elevation at 2 hours ($p=6.46 \times 10^{-5}$) and a 33% increase at 4 hours (9,917±475 RFU vs 13,194±1,129 RFU, p=0.0003). Co-administration with the cannabinoid receptor inhibitor rimonabant ameliorated the AEA-induced elevation in glucose, underscoring the specificity of the observations (Figure 7B, right panel).

In zebrafish, adipocytes do not develop until 12 dpf. However, younger zebrafish larvae have a characteristic pattern of lipid deposition which can be visualized with the fat soluble dye, Oil Red O. Typically, unfed larvae display low levels of neutral triglycerides and lipids in the central nervous system and yolk sac. The baseline level of lipid deposition was represented by 6 dpf control larvae (Figure 7C, top left panel). In contrast, larvae incubated with AEA displayed an increased amount of Oil Red O staining in several organ regions that was inhibited by co-administration of rimonabant (Fig 7C), particularly the liver which demonstrated a dose-dependent increase in staining (Figure 7D, boxes). Concordant with that observation, AEA induced a 39% increase in triglyceride levels in zebrafish larvae (13.3±0.01 mg/dl vs. 18.5±0.01 mg/dl, p=0.001; Figure 7E). The effect of AEA administration was not exclusive to the liver. Additional organ areas were also detected with Oil Red O, including the brain and vascular system (Figure 7F). Within the brain, Oil Red O staining was prominent in the diencephalon (Figure 7F, arrowheads) and the optic tectum. Within the vascular system of fish treated with AEA, the dorsal aorta, axial vein and intrasegmental blood vessels (Figure 7F, arrows) were enriched with lipid deposits compared to the absence of vascular lipid deposits in vehicle-treated control larvae.

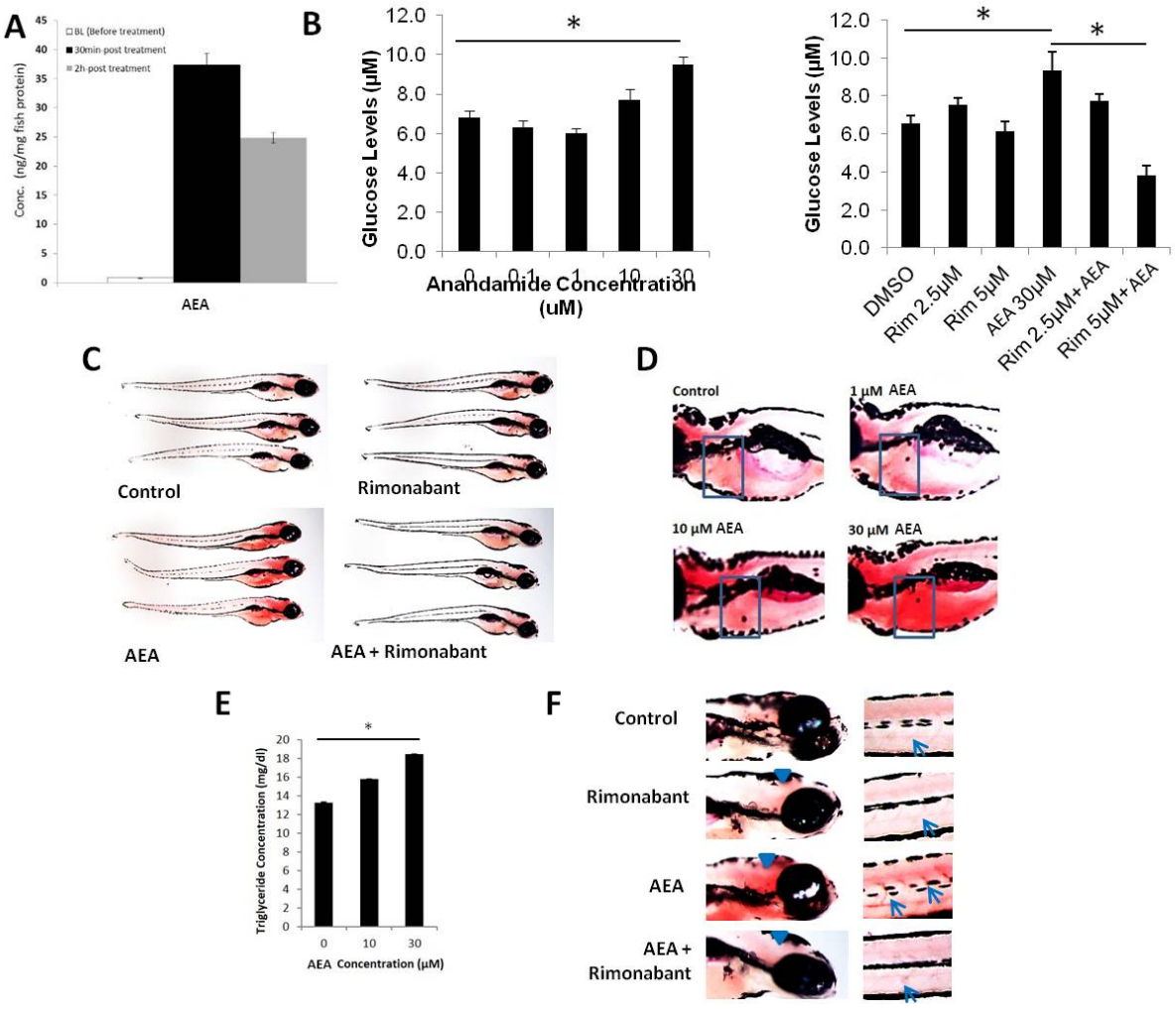

Supplemental Figure 7. Exogenous anandamide administration in zebrafish alters glucose levels and lipid accumulation. A) The concentration of AEA achieved within the fish was measured by comparing to deuterated anandamide-d_4, normalized to total fish protein. AEA, anandamide. **B)** Glucose levels were measured in 6 dpf larvae 4 hours post treatment with the increasing concentration of AEA in the water. Glucose was also measured in the presence of rimonabant, a cannabinoid receptor inhibitor. *, $p<0.001$; Glucose measurements provided in uM concentration; AEA, anandamide; Rim, rimonabant; data are mean±SEM. **C)** 6 dpf larvae stained with Oil Red O viewed laterally. **D)** Magnified views of the zebrafish, with the liver visualized by turning the fish to the left side. The location of the liver is shown by the blue box. **E)** Triglyceride concentration was measured in whole zebrafish larvae after treatment with increasing doses of AEA. *, $p=0.001$. **F)** Additional areas of AEA-dependent lipid staining included the brain (arrowheads) and the intersegmental vessels (arrows).

References

1. Annesley, T.M. Ion suppression in mass spectrometry. *Clinical chemistry* **49**, 1041-1044 (2003).
2. Dunn, W.B.*, et al.* Procedures for large-scale metabolic profiling of serum and plasma using gas chromatography and liquid chromatography coupled to mass spectrometry. *Nature protocols* **6**, 1060-1083 (2011).
3. Van Belle, G. & Martin, D.C. Sample size as a function of coefficient of variation and ratio of means. *The American Statistician* **47**, 165-167 (1993).
4. Wang, T.J.*, et al.* Metabolite profiles and the risk of developing diabetes. *Nat Med* **17**, 448-453 (2011).
5. Rhee, E.P.*, et al.* Lipid profiling identifies a triacylglycerol signature of insulin resistance and improves diabetes prediction in humans. *J Clin Invest* **121**, 1402-1411 (2011).
6. Rhee, E.P.*, et al.* A genome-wide association study of the human metabolome in a community-based cohort. *Cell Metab* **18**, 130-143 (2013).
7. Kimberly, W.T., Wang, Y., Pham, L., Furie, K.L. & Gerszten, R.E. Metabolite profiling identifies a branched chain amino acid signature in acute cardioembolic stroke. *Stroke; a journal of cerebral circulation* **44**, 1389-1395 (2013).